Journal of the European Ceramic Society 39 (2019) 1860–1868

Contents lists available at ScienceDirect

Journal of the European Ceramic Society

journal homepage: www.elsevier.com/locate/jeurceramsoc

Original Article

Combined effect of internal and external factors on sintering kinetics of plasma-sprayed thermal barrier coatings

Guang-Rong Li[a,b], Li-Shuang Wang[c], Guan-Jun Yang[a,*], Cheng-Xin Li[a], Chang-Jiu Li[a]

[a] State Key Laboratory for Mechanical Behavior of Materials, School of Materials Science and Engineering, Xi'an Jiaotong University, Xi'an, 710049, China
[b] State Key Laboratory for Manufacturing Systems Engineering, School of Mechanical Engineering, Xi'an Jiaotong University, Xi'an, 710049, China
[c] School of Materials Science and Engineering, Xi'an Shiyou University, Xi'an, 710065, China

ARTICLE INFO

Keywords:
Thermal barrier coatings
Scale-progressive evolution
Temperature-dependent sintering kinetics
Multiple contacts
Plasma spraying

ABSTRACT

Understanding the sintering kinetics of plasma-sprayed thermal barrier coatings (PS-TBCs) is crucial to retard their performance degradation. However, under real service condition, the sintering kinetics is often affected by multiple factors. This study investigated the sintering kinetics, in a novel scale-progressive view, under the combined-effect of internal and external factors. Results show that the sintering kinetics of PS-TBCs was highly associated with their unique sintering process from nanoscale to microscale. Firstly, sintering leads to nanoscopic roughening of the pore surface. Subsequently, multiple contacts are formed between counter-surfaces. As a result, microscopic healing of pores can be finally observed. In terms of external factors, the temperature further affects the level and rate of nanoscopic roughening. This is responsible for the differences of the microscopic healing ratios, as well as the macroscopic elastic modulus.

1. Introduction

Thermal barrier coatings (TBCs) offer protective function against high temperatures, which exceed the bearable limit of the underlying components (often made of superalloy) in aircraft engines and land-based gas turbines [1–8]. Therefore, consistently high thermal insulation and durable service lifetime are crucial for TBCs. Plasma spraying has proven its benefit for preparing TBCs with excellent thermal barrier performance [9–14]. This is primarily attributed to the lamellar structure formed from the stacking of re-solidified splats [15]. In addition, the strain tolerance of plasma-sprayed TBCs is enhanced distinctly with respect to the bulk materials [16–20]. As a result, plasma-sprayed TBCs find their widely application in gas turbine.

During thermal exposure, TBCs undergo inevitable structural changes, along with performance degradation [21–24]. This is very common for defect-rich ceramic structures affected by sintering. The sintering process threatens TBCs mainly in the following ways: (i) the thermal conductivity is increased significantly, suggesting that the thermal barrier performance is weakened [9,25]; (ii) the coating stiffens, and the strain tolerance capacity is thereby decreased [26–28]. Moreover, the latter promotes the formation of large-scale cracks, which are responsible for the failure phenomenon caused by spallation [19,29–31]. Overall, sintering leads to performance degradation of TBCs. It is suggested that the property changes are highly associated with the specific microstructural evolution. In conventional porous ceramic structures, porosity is often used to characterize the essential structural changes, since the voids are often 3-dimensional [32,33]. In contrast, in plasma-sprayed TBCs, changes in inter-splat pores and intra-splat cracks dominate the microstructural evolution [20]. These pores and cracks have much larger dimensions (approximately several micrometers to several tens of micrometers) in two directions than that in the third direction (approximately several nanometers to several tens of nanometers), thus they can be regarded as 2-dimensional (2D) pores or cracks [34–36]. This is the reason that the decrease of apparent porosity is less than 20%, whereas the increases in thermal conductivity and elastic modulus are over 100% [18]. Some authors have presented direct experimental observations of sintering-induced healing of 2D pores [37]. Others confirmed the dominant role of 2D pores from a statistical viewpoint [5,38]. Generally, sintering-induced performance degradation is primarily caused by the healing of 2D pores (or cracks).

However, sintering is a thermally-activated process, which means that the healing of 2D pores would be spontaneous if the TBCs were exposed to high temperatures. Therefore, sintering kinetics is critically important, since it is essential to find ways to retard performance degradation. In our previous reports [28,39], sintering kinetics as a function of heating duration was presented, along with a quantitative analysis which related the mechanical properties and microstructure. It is suggested that ultrafast sintering kinetics occurs during the initial

* Corresponding author.
E-mail address: ygj@mail.xjtu.edu.cn (G.-J. Yang).

https://doi.org/10.1016/j.jeurceramsoc.2018.12.053
Received 23 May 2018; Received in revised form 16 December 2018; Accepted 21 December 2018
Available online 23 December 2018
0955-2219/

stage, followed by much slower rates at extended durations. Similar results on sintering kinetics affected solely by heating duration can also be found in other reports [9,16,25]. Nevertheless, the previous work does not cover all the cases of sintering kinetics that occurs in real service. On one hand, TBCs often must work at various temperatures depending on the process requirements. On the other hand, the next generation of TBCs should have the ability to withstand higher temperatures, so that a higher efficiency can be obtained from gas turbines [40]. All these points suggest that sintering kinetics dependent on both temperature and dwell time would be crucial for current use and the future development of TBCs.

Therefore, the objective of this work is to investigate the co-effect of temperature and dwell time on the sintering kinetics of plasma-sprayed TBCs. The changes of structure investigated primarily are the healing rates of 2D pores, whereas the properties are determined at multiple scales. First, samples were exposed to different temperatures for hundreds of hours. During the process, changes of microstructure were characterized, and the properties in multiple scales were determined. Subsequently, a structural model was used to correlate the changes of microstructure and the mechanical properties, to identify the dominant factors controlling the sintering kinetics. Next, the temperature-sensitive rates of 2D pore healing were analysed in detail. This study provides a comprehensive understanding of the sintering kinetics of plasma-sprayed TBCs.

2. Experimental procedure

2.1. Sample preparation

A commercially available hollow spherical 8 wt.% YSZ powder (HOSP, -75 to + 45 μm, Metco 204B-NS, Sulzer Metco Inc., New York, USA) was used to deposit ceramic coatings with a commercial plasma spray system (GP-80, 80 kW class, Jiujiang, China). The plasma spraying parameters are shown in Table 1. The thickness of the top coat was approximately 500 μm. In this study, all samples to be exposed were in their free-standing states. Therefore, stainless steel was used to support the coating deposition. To represent the geometries of different applications, substrates were designed to have either a circular shape with dimensions φ20 mm × 3 mm or a rectangular shape with dimensions 60 mm × 10 mm × 3 mm. Grit blast was used to roughen the substrate, to ensure good adhesion between the coating and substrate. Subsequently, a hydrochloric acid solution was used to remove the steel substrates.

2.2. Thermal exposure of samples

The service temperature of TBCs is often above 1000 °C. Therefore, 3 different temperatures of thermal exposure were selected, 1000 °C, 1200 °C, and 1400 °C. At each temperature, evolution as a function of dwell time was investigated. Therefore, the co-effect of temperature and durations on the sintering kinetics can be obtained. Relatively low heating and cooling rates of 10 °C/min were used.

Table 1
Parameters used for PS-YSZ coatings.

Parameter	Unit	Value
Plasma arc voltage	V	70
Plasma arc current	A	600
Flow rate of primary gas (Ar)	L/min	50
Flow rate of secondary gas (H_2)	L/min	7
Flow rate of powder feeding gas (N_2)	L/min	7
Spray distance	mm	110
Torch traverse speed	mm/s	800

2.3. Microstructural characterization

Healing of 2D pores was observed using scanning electron microscopy (SEM, TESCAN MIRA 3, Brno, Czech Republic). The circular shaped samples (φ20 mm × 0.5 mm) were used for the in-situ observation. The detailed procedure can be found elsewhere [28], but the general procedure is as follows: (i) a target inter-splat pore is found from the sample cross-sections at high magnifications; (ii) the magnification is decreased gradually to view the global morphology of the sample; (iii) the target position is determined by fixing the corresponding coordinates; (iv) the target can be re-located after thermal treatment according to its coordinates.

The healing behaviour of 2D pores was also investigated in a statistical way. Because pores are 2D, their healing behaviour can be characterized by the total pore length per unit area, called the length density. The statistical length was determined under a magnification of 5000× using SEM. For micropores that were difficult to measure, a higher magnification was used. The densities of inter-splat pores were measured at polished cross-sections, whereas the coating surface provided the area to determine the densities of intra-splat cracks. At each state during thermal exposure at different temperatures, at least 50 SEM images were analysed.

An inter-splat pore is actually unbonded interface between two neighbouring splats. Therefore, the inter-splat pores are formed by the top and bottom surfaces of two splats. Thus, the change of the splat surface was used to investigate the healing rate at different temperatures. Atomic force microscopy (AFM, Asylum Research Cypher, USA) was used to characterize the surface changes of the splats. In addition, high resolution transmission electron microscopy (HRTEM, JEM-2100 F, JEOL, Japan) was used to observe the pore healing behaviour.

2.4. Determination of mechanical properties in multiple scales

Because defects are multiscale, the mechanical properties of plasma-sprayed ceramic coatings often appear to be scale-sensitive [41]. Therefore, it is necessary to determine the mechanical properties of plasma-sprayed TBCs at multiple scales. For the microscale elastic modulus, the Knoop indentation test (Buehler Micromet 5104, Akashi Corporation, Japan) was used with a test load of 300 gf and a holding time of 30 s. The circular samples (φ20 mm × 0.5 mm) were used to determine the microscopic elastic modulus. For the macroscopic elastic modulus, rectangular samples (60 mm × 10 mm × 3 mm) were used with a three-point bending test (Instron 5943, America). The multiscale elastic moduli of samples were determined only in their in-plane directions, since the strain generated during thermal service is mainly along the coating surface [18].

3. Results

3.1. Changes of elastic modulus in multiple scales dependent on temperatures

Fig. 1 shows changes of the elastic modulus as a function of dwell time at different temperatures. It is found that the sintering kinetics is featured with two stages on double logarithmic plots. Fig. 2 shows the increments of elastic modulus at different stages, which are defined according to the turning points of the slope values. Table 2 shows the slope values of the different linear portions. The dwell time of stage I at 1400 °C, 1200 °C, and 1000 °C is approximately 6 h, 10 h, and 20 h, respectively. Some similar trends were observed for all the temperatures, as seen in Figs. 1 and 2. First, the overall rates of change were divided into two stages approximately, confirming that the sintering kinetics is time-sensitive. During the initial stage (called stage I) of several hours, the sintering kinetics appears to be ultrafast. However, during the following extended stage (called stage II), the increasing rates slow down significantly. Second, the increments during the stage I

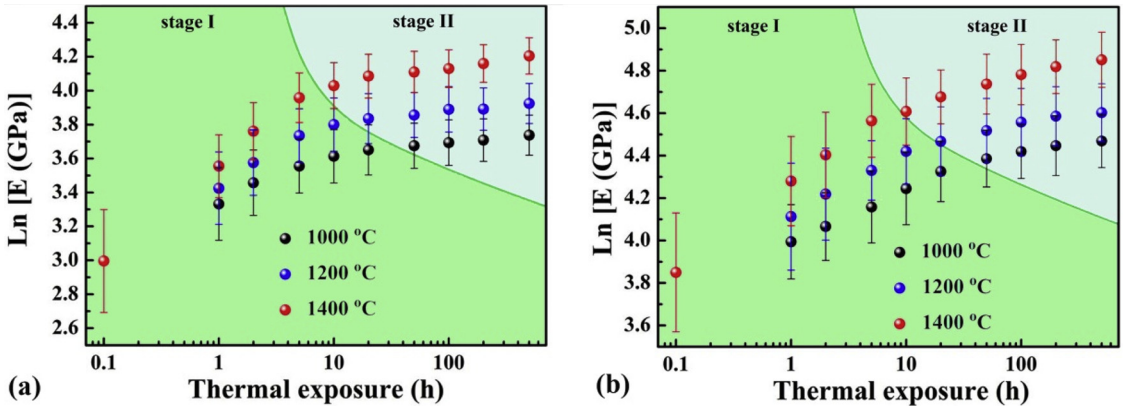

Fig. 1. Changes of elastic modulus during thermal exposure on double logarithmic plots: (a) macroscale and (b) microscale.

are much larger than those during the stage II.

In addition to the above-mentioned similar phenomena caused by dwell time, a significant effect of temperature on sintering kinetics can also be found. First, a higher temperature leads to a faster rate of change during the stage I. Moreover, the increase of the changing rate seemed to be gradual from 1000 °C to 1200 °C. However, a sharp increase was observed from 1200 °C to 1400 °C. These suggest that the effect of temperature on sintering kinetics is enhanced distinctly at higher temperature. Second, the increments of samples during stage I were increased with the temperature. Thirdly, it was found that a higher temperature completes its first stage in shorter time. Overall, from the changes of the elastic modulus, it was found that higher temperatures result in faster sintering kinetics, and this effect is enhanced above 1200 °C.

3.2. Changes of 2D pore density

Fig. 3 shows the changes of 2D pores as a function of dwell time at different temperatures. Fig. 4 shows the decrement of 2D pore density at different stages. Similar to the mechanical properties, the effects of dwell time and temperature on the healing rates of 2D pores are obvious. It was found that the healing rates of inter-splat pores and intra-splat cracks have different dependencies on the dwell time. The inter-splat pore densities decreased significantly during the stage I. In contrast, the intra-splat cracks showed a slight decrease in pore density during the stage I, albeit at a much higher rate during the stage II. Regarding the effect of temperature, it was found that the healing rate of inter-splat pores increased at higher temperatures. Moreover, with the increase of temperature, a shorter stage I can lead to a larger decrement of inter-splat pore density.

Table 2
Slope values of the different linear portions of elastic modulus obtained from Fig. 1.

	Stage I		Stage II	
	Macroscale	Microscale	Macroscale	Microscale
1000 °C	0.03	0.02	0.0001	0.0003
1200 °C	0.08	0.06	0.0002	0.0004
1400 °C	0.17	0.12	0.0004	0.0005

3.3. Correlation between microstructure and mechanical properties

In Figs. 1 and 3, similar temperature effects on sintering kinetics can be seen. Therefore, it is necessary to correlate the changes of the microstructure and mechanical properties. A structural model was developed to predict the in-plane elastic modulus and the effect of the healing of 2D pores, as shown in Fig. 5. A plasma sprayed coating is formed by the stacking of splats re-solidified from molten powders. Due to the brittle feature of ceramic materials, the original disk-shaped splats are fractured into several segments under the quenching stress [35]. Therefore, plasma-sprayed ceramic coatings are actually stacks of those segments. Along the through-thickness direction, the segments are bonded partially, resulting in the formation of inter-splat pores. Along the in-plane direction, the segments are divided by intra-splat cracks [34]. The assumptions are described as follows: (i) the segments are all assumed to be cubic, despite their irregular initial shapes; (ii) the bonding areas are located at the bottom center of the segments; (iii) the stacking of structural units is uniform. The healing of 2D pores is realized by bonding their counter surfaces. The bonding ratio at different dwell time is obtained from the corresponding changing ratio of 2D pore density.

The elastic modulus was predicted using the commercial FEM code

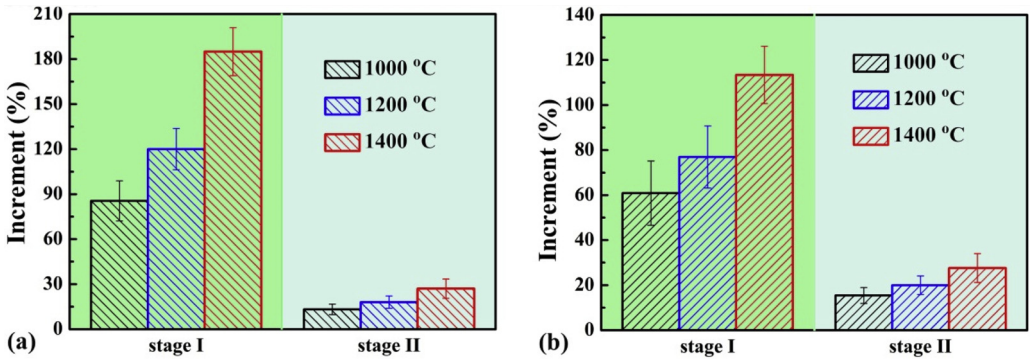

Fig. 2. Increments of elastic modulus at different stages: (a) macroscale and (b) microscale.

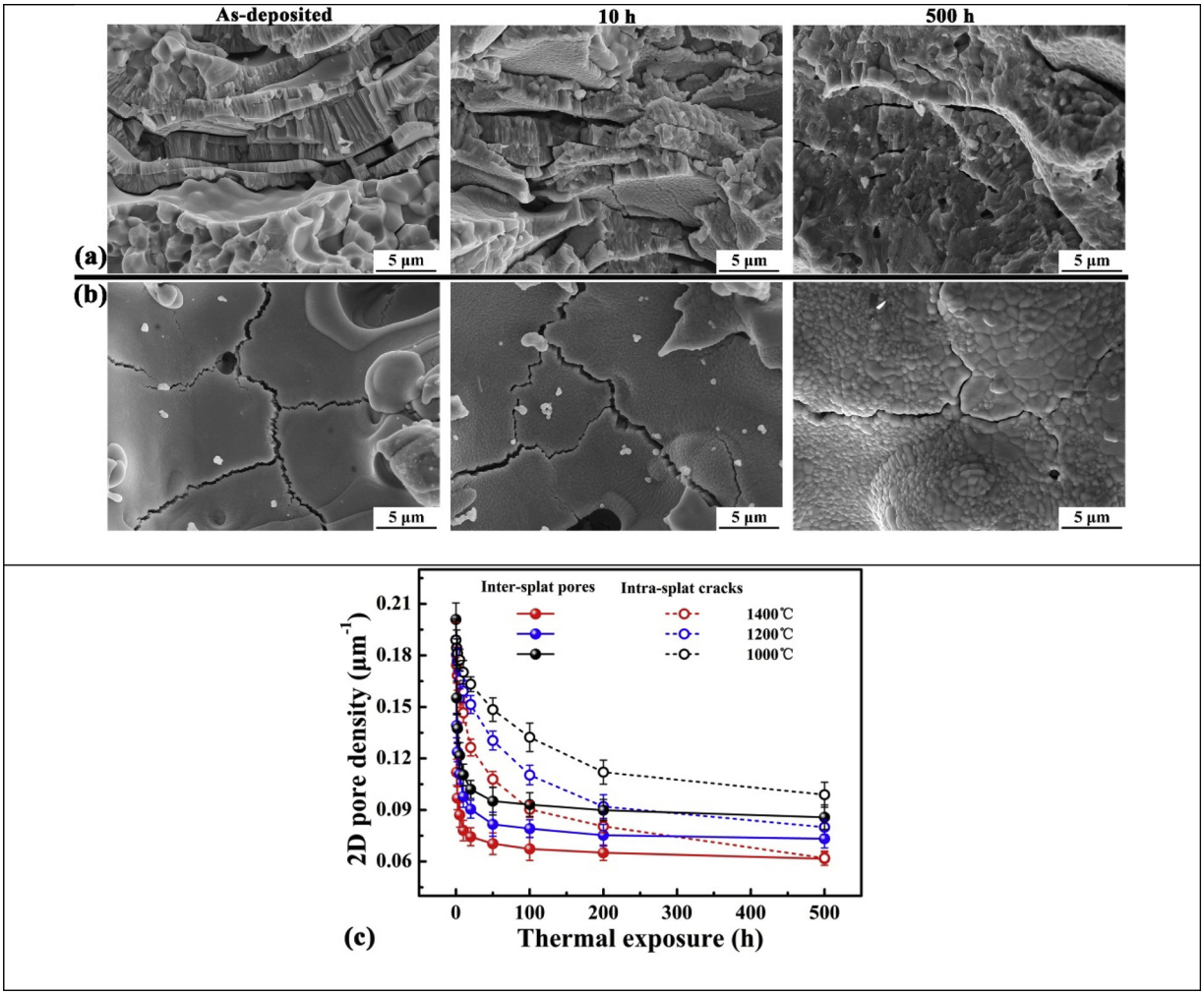

Fig. 3. Changes in 2D pores during thermal exposure: (a) fractured cross sections of samples at different dwell time of 1200 °C, (b) sample surface at different dwell time of 1200 °C, and (c) 2D pore density as a function of dwell time at different temperatures.

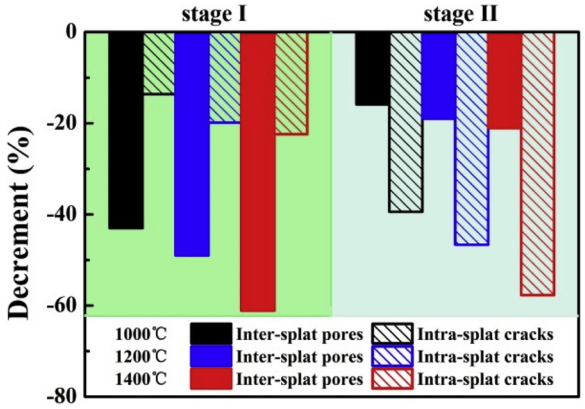

Fig. 4. Decrements of 2D pore density at different stages.

ABAQUS. A periodic pattern was extracted by cutting splat segments in lower layers along the segment boundaries in upper layer, as shown in Fig. 5. As a result, the periodic pattern is formed by stacking of two layers: a whole splat segment from upper layer and four parts of four splat segments in the lower layers. Periodic boundary conditions were applied on the corresponding-pair surfaces, so that they would behave consistently under load. In this way, the intrinsic elastic modulus of the structure can be determined using the periodic pattern, which eliminates the need to consider the dimensions of the entire surface. The details for introducing periodic boundaries can be found elsewhere [42]. Herein, the segment is set to be homogeneous, isotropic, and linearly elastic. Other parameters can be found in Table 3. The x–z plane is taken as the reference plane (in-plane direction), which is perpendicular to the heat flux. To obtain the elastic modulus, a tensile strain along the in-plane direction was applied to the cross-section with periodic boundary conditions. Subsequently, the stress-strain curve can be used to determine the elastic modulus.

Fig. 6 shows the predicted elastic modulus as a function of splat length and thickness, along with experimental data determined by Knoop indentation. The elastic modulus is found to be linearly affected by the length and thickness of splat segments. Therefore, it would be reasonable to use average value for the final prediction, as shown in Fig. 6c. It is found that the predicted elastic moduli are consistent with the trends of the experiments. The overall dwell time is divided into two stages for all temperatures. It was found that higher temperatures lead to a faster and larger increase of the elastic modulus during stage I.

In summary, the correlation between the microstructure and mechanical properties suggests that the healing of 2D pores is primarily responsible for the performance degradation. This is consistent with previous reports [28,36]. Therefore, the sintering kinetics of plasma-sprayed TBCs corresponds to the healing rate of 2D pores. The effects of internal and external factors on healing rate were discussed in the following sections.

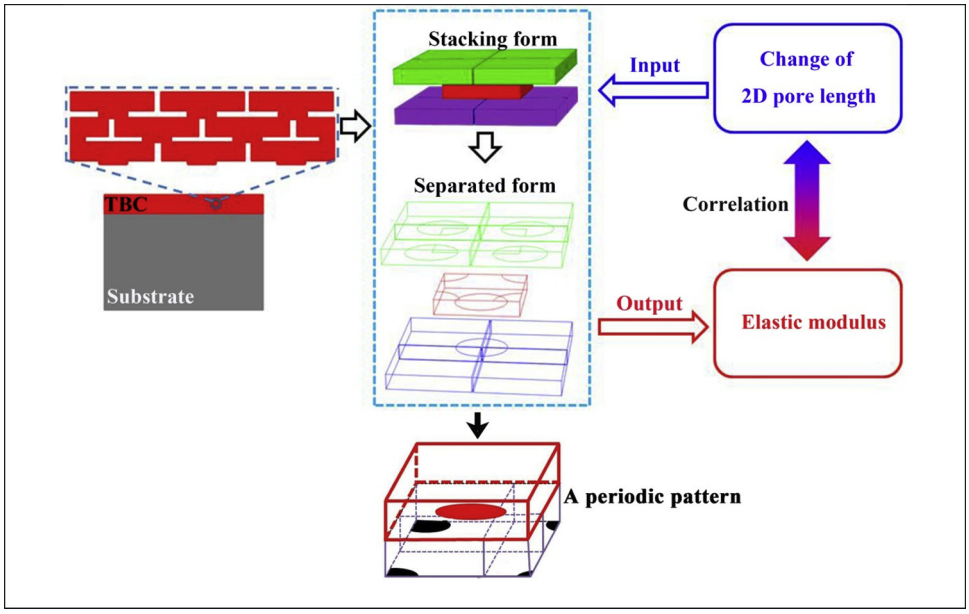

Fig. 5. Development of structural model to correlate elastic modulus with 2D pores.

Table 3
Parameters of model to predict elastic modulus.

Classification	Parameters	Values
Material intrinsic properties	Young's modulus	205 GPa
	Possion's ratio	0.23
Structure	Splat length	6~15 μm
	Splat thickness	1~2 μm
	Initial bonding ratio	28%
Model	Global seeds for meshing	0.2 μm
	Global strain	0.02%

4. Discussion

It was found from Fig. 2 that the increase of elastic modulus during the stage I is often above 70% of the total change. Correspondingly, during stage I, the dominant structural change is the healing of inter-splat pores (see Fig. 4). Therefore, to retard the performance degradation, the mechanism of the temperature dependence of the healing rates of inter-splat pores is critically important.

4.1. Internal factor: scale-progressive healing mechanism of inter-splat pores

Commonly, sintering of ceramics is a result of thermally activated

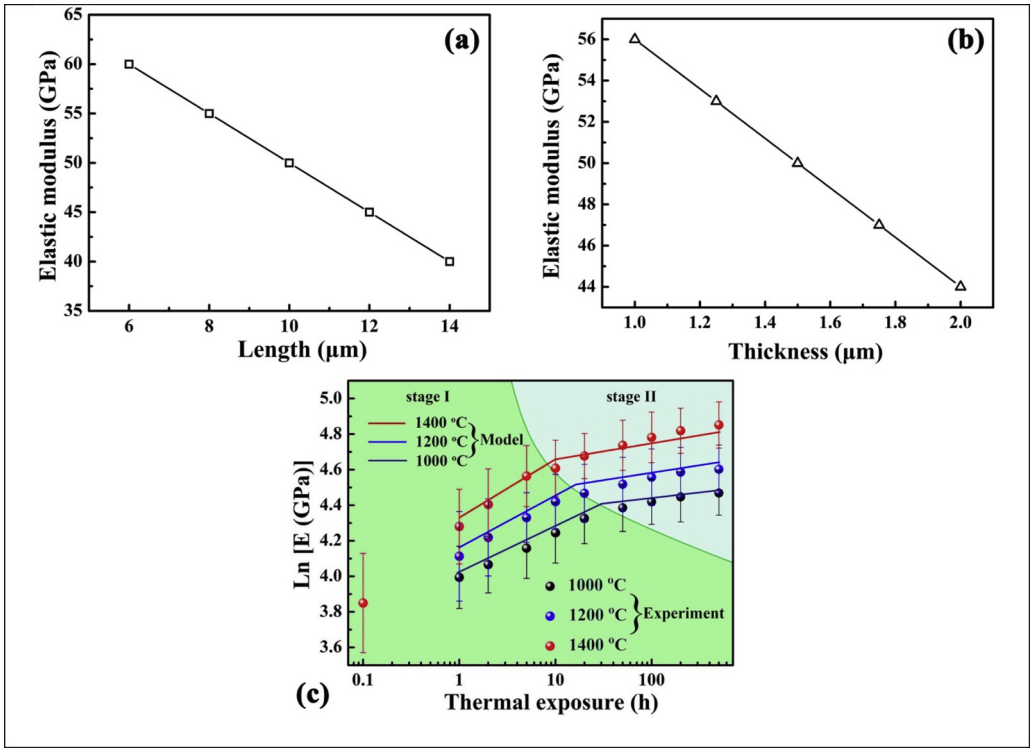

Fig. 6. Predicted elastic modulus as a function of splat length (a) and thickness (b); and (c) comparison between model prediction and experimental results.

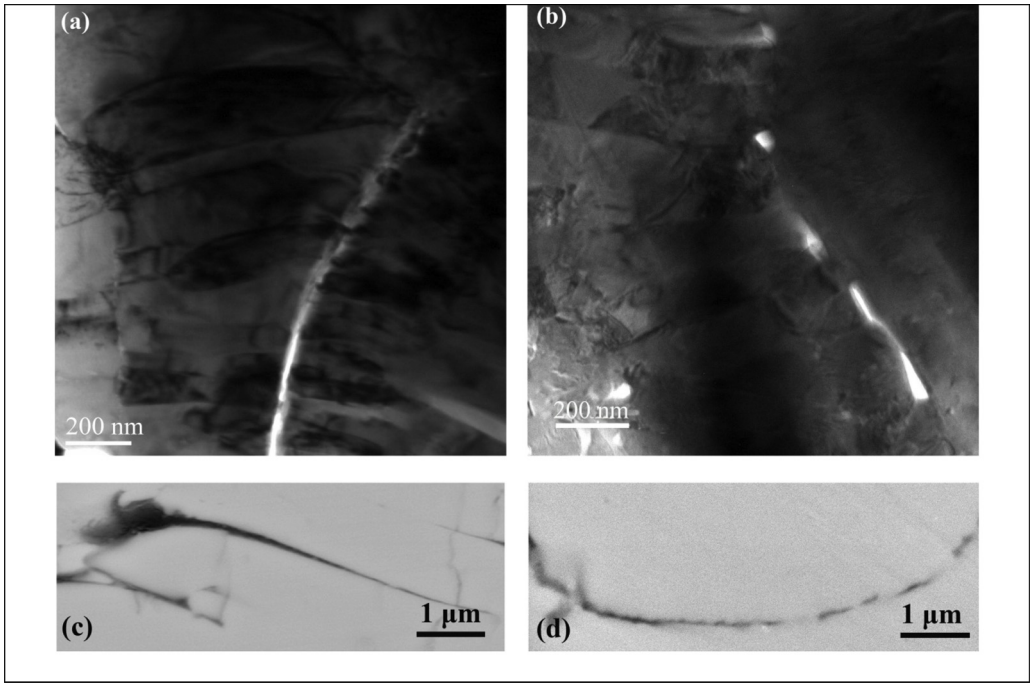

Fig. 7. Multiple contact healing behaviour of inter-splat pores by TEM and SEM: (a) and (c) are initial states; (b) and (d) are states after thermal exposure at 1200 °C for 20 h.

matter transfer, to decrease the free energy of whole system. For example, during the sintering of ceramic powders, a neck between powders is formed followed by its diameter growth [43]. For plasma-sprayed TBCs, the pore surface would similarly decrease due to healing. However, the healing process is structure specific. In plasma-sprayed TBCs, the inter-splat pores are formed due to partially bonded splats. Cipitria et al. [34] developed a structural model to investigate the sintering process. In their model, the healing of inter-splat pores occurred due to the diameter increase of the bonding area at a constant rate. They guided the investigation of sintering behaviour from the view of pore healing. However, their predicted results cannot capture the ultrafast sintering kinetics observed during the stage I. This suggests that the healing mechanism of inter-splat pores may be different from our conventional understanding. Fig. 7 shows the healing behaviour of inter-splat pores characterized by TEM and SEM. A common phenomenon is that the pores evolve from a continuous to a separated morphology. It seems that the pores are bridge-connected in some areas. This suggests that, in addition to gradual increase in bonding area, multiple contacts occurred during the healing of inter-splat pores. The multiple contacts are the essential cause of the ultrafast sintering kinetics during stage I. During sintering, the healing of pores occurs through matter transfer. Therefore, the healing rate of inter-splat pores is determined by the transfer rate of matter. The multiple contacts formed between inter-splat pores provide more paths to transfer matter simultaneously. As a result, the sintering kinetics driven by the multiple contact paths are much higher than that of the single path assumed in previous report [34].

The multiple contacts in 2D gaps (i.e., an inter-splat pore) are mainly caused by the combined effect of roughening in the splat surface and the morphology of inter-splat pores. The roughening effect is also reported in previous papers with different materials, like YSZ [39,44] and $La_2Zr_2O_7$ [45]. Fig. 8 shows the morphology change of a splat surface. It is seen that the initial smooth surface roughens in nanoscale after thermal exposure. It is reported that the dominant diffusion mechanism at 1000 °C is surface diffusion, whereas it is volume diffusion at 1200 °C and above [46]. In addition, the volume diffusion would cause densification, as well as changes in macroscopic dimensions [34].

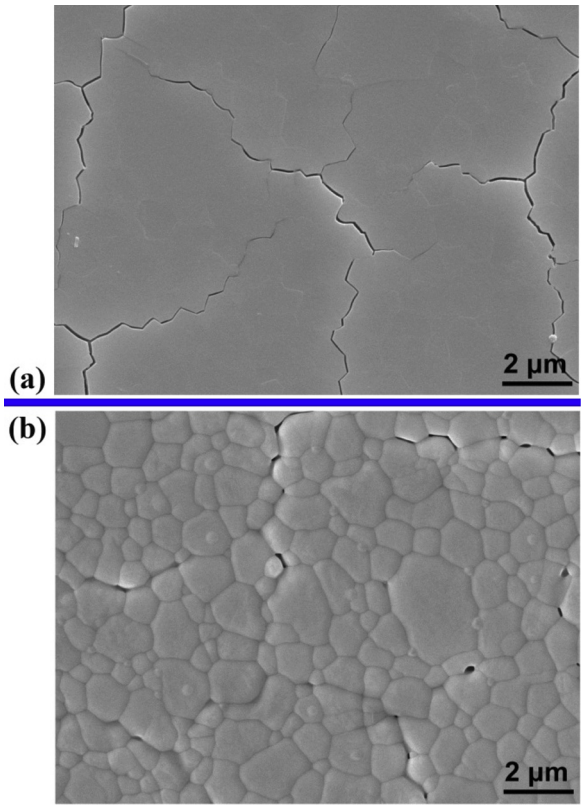

Fig. 8. Morphology change of splat surface at 1200 °C: (a) as-deposited state and (b) after thermal exposure.

Therefore, the roughening in Fig. 8 is mainly caused by volume diffusion. Regarding the effect of splat morphology, their width appears to be non-equal (see Fig. 7c). At the narrow area, the effect of nanoscale roughening can cause multiple contacts of the counter-surfaces of an inter-splat pore in microscale (see Fig. 7). Subsequently, the healing of

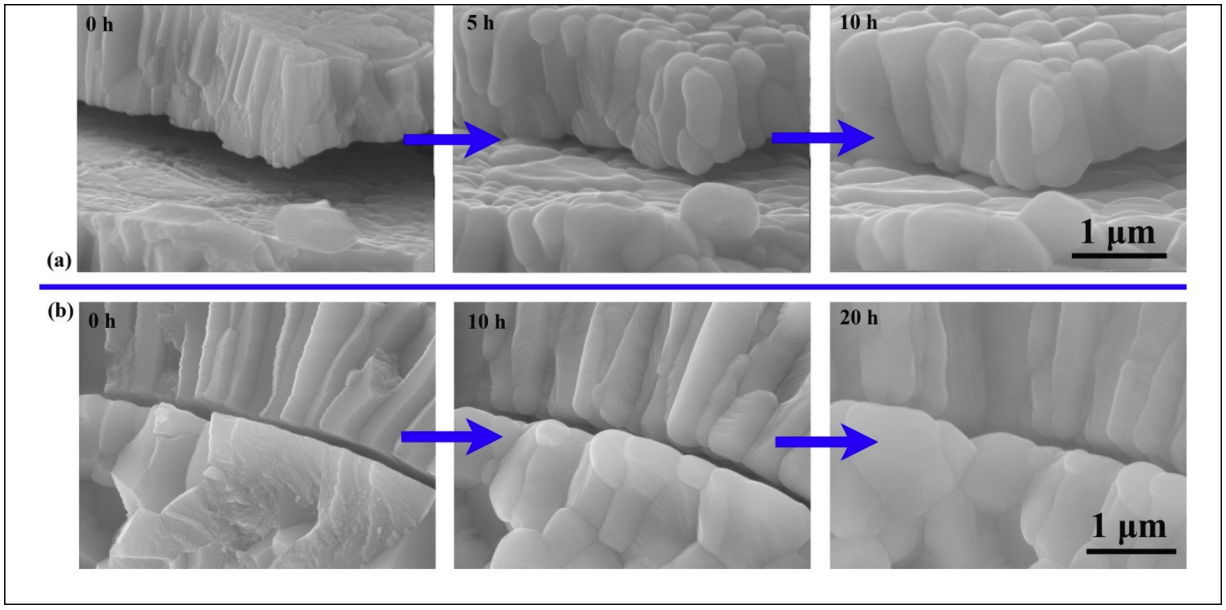

Fig. 9. Quasi in-situ observation of healing of inter-splat pores: (a) 1400 °C, (b) 1200 °C.

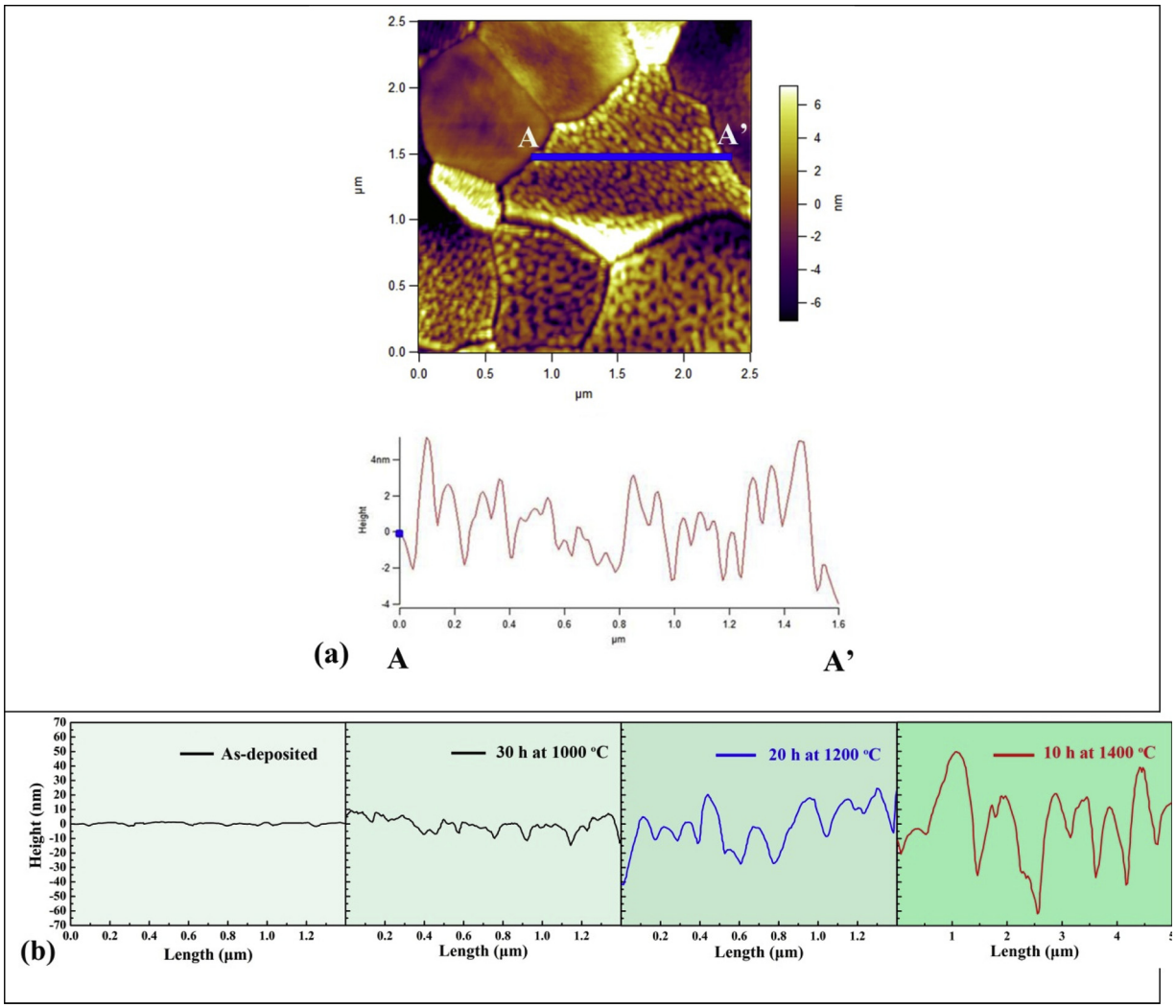

Fig. 10. Temperature-dependent changes of surface height after thermal exposure: (a) method to obtain surface height by AFM, (b) comparison for different temperatures.

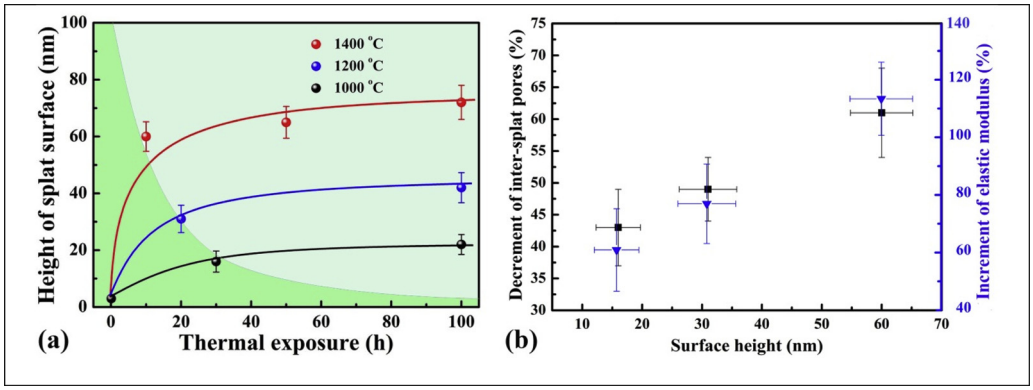

Fig. 11. Sintering kinetics affected by internal and external factors: (a) surface height as a function of dwell time at different temperatures, (b) relationship between surface height and pore healing and elastic modulus.

inter-splat pores proceeds by the sintering of contacted-grains. This is consistent with the previous report [46]. The whole process is accompanied by a diameter increase of the contact-neck, just like the sintering mechanism of ceramic powders [43]. In summary, the healing pattern of inter-splat pores occurs due to having multiple contacts in a narrow area, which is related to the material and structure.

4.2. External factor: temperature-dependent sintering kinetics of plasma-sprayed TBCs

Based on the healing mechanism described above, the sintering kinetics of plasma-sprayed TBCs will be highly related to the healing rate of inter-splat pores. As a result, the roughening scale and rate would be the two main factors that affect the sintering process. Fig. 9 shows the quasi in-situ healing of inter-splat pores at different temperatures. The pore surfaces roughen at all temperatures, which is consistent with the AFM result (see Fig. 8). However, taking the temperature effect into account, the roughening features are obviously different. Fig. 10 shows the surface height after thermal exposure at different temperatures. The dwell time approximately correspond to stage I. Firstly, the roughening scales are different. At 1400 °C, the height of the splat surface can be above 60 nm, whereas it is less than 20 nm at 1000 °C. There is no doubt that a larger height of the surface roughening would lead to more contact area or a higher healing ratio [39]. This can be responsible for the larger increment of the elastic modulus at higher temperature (see Fig. 2), since the properties of plasma sprayed ceramic coatings are determined mainly by the bonding ratio [35,47]. Moreover, the healing pattern of multiple contacts gives an equal healing chance for the contacted area. This means that a higher healing ratio often corresponds to a faster increase-rate of the elastic modulus. Secondly, the mechanism of matter transfer is dependent on the temperature [46]. A higher temperature results in a larger driving force for matter transfer. Consequently, at a higher temperature, the roughening of the splat surface can reach its stable state earlier. This is the reason that the stage I duration with ultrafast sintering kinetics becomes shorter with an increase of temperature (see Fig. 1).

The sintering kinetics of plasma sprayed TBCs, affected by temperature and dwell time, are shown in Fig. 11. The changes of surface height as a function of dwell time are obviously non-linear (Fig. 11a). Moreover, the temperature enhanced this non-linear behaviour. As a result, the increased scale and rate of the surface roughening is significantly improved. The healing of inter-splat pores, as well as the increase of elastic modulus is relatively linearly related to surface height (Fig. 11b). The reason is that the multiple contact healing behaviour of inter-splat pores dominates the sintering during stage I with ultrafast kinetics. The temperature affects the roughening scale and rate (Fig. 11a). Therefore, it can be concluded that the healing rate of inter-splat pores and the increase rate of mechanical properties are highly dependent on the temperature and dwell time. This is the main mechanism responsible for the sintering kinetics involving a combined effect of internal and external factors.

5. Conclusions

In this study, the sintering kinetics, affected by internal and external factors, of the PS-TBCs were investigated in a novel scale-progressive view. The unique internal sintering behaviour is primarily responsible for the external temperature effect on sintering kinetics. The detailed conclusions are as follows:

(i) In terms of internal factors, the sintering is associated with the changing features of the materials and structure. First, the pore surfaces evolve due to nanoscopic roughening from an initially smooth surface. Subsequently, the roughened surface leads to multiple contacts between the counter-surfaces of the inter-splat pores. Finally, microscopic healing can be observed. The whole process proceeds due to matter transfer, accompanied by a decrease of free energy. This healing mechanism with multiple contacts is responsible for the time-sensitive sintering kinetics.
(ii) In terms of external factors, the temperature affects the level and rate of nanoscopic roughening at the pore surface. As a result, a higher temperature leads to a larger microscopic healing ratio in shorter time. This is the essential cause of the differential increments of the elastic modulus in multiple scales.

Finally, the combined effect of internal and external factors on sintering kinetics provides a comprehensive understanding on the structural evolution of the plasma-sprayed TBCs. This is essential for the further structural tailoring of TBCs to retard their performance degradation and to develop advanced TBCs with higher performance.

Acknowledgments

This work was supported by the National Natural Science Foundation of China (grant number 51801148); the China Postdoctoral Science Foundation (grant number 2018M631151); the Equipment Advance Research Foundation (grant number 61409220117); the National Basic Research Program of China (grant number 2013CB035701); the Fundamental Research Funds for the Central Universities; and the National Program for Support of Top-notch Young Professionals.

References

[1] R. Vassen, A. Stuke, D. Stover, Recent developments in the field of thermal barrier coatings, J. Therm. Spray Technol. 18 (2) (2009) 181–186.
[2] N.P. Padture, Advanced structural ceramics in aerospace propulsion, Nat. Mater. 15

(8) (2016) 804–809.
[3] N.P. Padture, M. Gell, E.H. Jordan, Materials science - Thermal barrier coatings for gas-turbine engine applications, Science 296 (5566) (2002) 280–284.
[4] A. Ganvir, S. Joshi, N. Markocsan, R. Vassen, Tailoring columnar microstructure of axial suspension plasma sprayed TBCs for superior thermal shock performance, Mater. Design 144 (2018) 192–208.
[5] G.R. Li, J. Lei, G.J. Yang, C.X. Li, C.J. Li, Substrate-constrained effect on the stiffening behavior of lamellar thermal barrier coatings, J. Eur. Ceram. Soc. 38 (6) (2018) 2579–2587.
[6] Z.L. Qu, K. Wei, Q. He, R.J. He, Y.M. Pei, S.X. Wang, D.N. Fang, High temperature fracture toughness and residual stress in thermal barrier coatings evaluated by an in-situ indentation method, Ceram. Int. 44 (7) (2018) 7926–7929.
[7] W.Z. Tang, L. Yang, W. Zhu, Y.C. Zhou, J.W. Guo, C. Lu, Numerical simulation of temperature distribution and thermal-stress field in a turbine blade with multilayer-structure TBCs by a fluid-solid coupling method, J. Mater. Sci. Technol. 32 (5) (2016) 452–458.
[8] L. Guo, M.Z. Li, Y. Zhang, F.X. Ye, Improved toughness and thermal expansion of non-stoichiometry $Gd_{2-x}Zr_{2+x}O_{7+x/2}$ ceramics for thermal barrier coating application, J. Mater. Sci. Technol. 32 (1) (2016) 28–33.
[9] S. Paul, A. Cipitria, S.A. Tsipas, T.W. Clyne, Sintering characteristics of plasma sprayed zirconia coatings containing different stabilisers, Surf. Coat. Technol. 203 (8) (2009) 1069–1074.
[10] E. Bakan, R. Vassen, Ceramic top coats of plasma-sprayed thermal barrier coatings: materials, processes, and properties, J. Therm. Spray Technol. 26 (6) (2017) 992–1010.
[11] M. Mutter, G. Mauer, R. Mucke, O. Guillon, R. Vassen, Systematic investigation on the influence of spray parameters on the mechanical properties of atmospheric plasma-sprayed YSZ coatings, J. Therm. Spray Technol. 27 (4) (2018) 566–580.
[12] G. Mauer, R. Vassen, Current developments and challenges in thermal barrier coatings, Surf. Eng. 27 (7) (2011) 477–479.
[13] M. Gupta, N. Curry, P. Nylen, N. Markocsan, R. Vassen, Design of next generation thermal barrier coatings - Experiments and modelling, Surf. Coat. Technol. 220 (2013) 20–26.
[14] G. Mauer, N. Schlegel, A. Guignard, M.O. Jarligo, S. Rezanka, A. Hospach, R. Vassen, Plasma spraying of ceramics with particular difficulties in processing, J. Therm. Spray Technol. 24 (1-2) (2015) 30–37.
[15] H. Xie, Y.C. Xie, G.J. Yang, C.X. Li, C.J. Li, Modeling thermal conductivity of thermally sprayed coatings with intrasplat cracks, J. Therm. Spray Technol. 22 (8) (2013) 1328–1336.
[16] J.A. Thompson, T.W. Clyne, The effect of heat treatment on the stiffness of zirconia top coats in plasma-sprayed TBCs, Acta Mater. 49 (9) (2001) 1565–1575.
[17] Y. Tan, A. Shyam, W.B. Choi, E. Lara-Curzio, S. Sampath, Anisotropic elastic properties of thermal spray coatings determined via resonant ultrasound spectroscopy, Acta Mater. 58 (16) (2010) 5305–5315.
[18] G.R. Li, G.J. Yang, C.X. Li, C.J. Li, Strain-induced multiscale structural changes in lamellar thermal barrier coatings, Ceram. Int. 43 (2) (2017) 2252–2266.
[19] G.R. Li, B. Cheng, G.J. Yang, C.X. Li, Strain-induced stiffness-dependent structural changes and the associated failure mechanism in TBCs, J. Eur. Ceram. Soc. 37 (11) (2017) 3609–3621.
[20] G.R. Li, G.J. Yang, C.X. Li, C.J. Li, Force transmission and its effect on structural changes in plasma-sprayed lamellar ceramic coatings, J. Eur. Ceram. Soc. 37 (8) (2017) 2877–2888.
[21] B. Cheng, G.J. Yang, Q. Zhang, N. Yang, M. Zhang, Y.M. Zhang, C.X. Li, C.J. Li, Gradient thermal cyclic behaviour of $La_2Zr_2O_7$/YSZ DCL-TBCs with equivalent thermal insulation performance, J. Eur. Ceram. Soc. 38 (4) (2018) 1888–1896.
[22] Y.X. Kang, Y. Bai, W. Fan, T. Yuan, Y. Gao, C.G. Bao, B.Q. Li, Thermal cycling performance of $La_2Ce_2O_7$/50 vol.% YSZ composite thermal barrier coating with CMAS corrosion, J. Eur. Ceram. Soc. 38 (7) (2018) 2851–2862.
[23] R. Vassen, S. Giesen, D. Stover, Lifetime of plasma-sprayed thermal barrier coatings: comparison of numerical and experimental results, J. Therm. Spray Technol. 18 (5-6) (2009) 835–845.
[24] E. Bakan, D.E. Mack, G. Mauer, R. Mucke, R. Vassen, Porosity-property relationships of plasma-sprayed $Gd_2Zr_2O_7$/YSZ thermal barrier coatings, J. Am. Ceram. Soc. 98 (8) (2015) 2647–2654.
[25] F. Cernuschi, P.G. Bison, S. Marinetti, P. Scardi, Thermophysical, mechanical and microstructural characterization of aged free-standing plasma-sprayed zirconia coatings, Acta Mater. 56 (16) (2008) 4477–4488.
[26] Y. Tan, J.P. Longtin, S. Sampath, H. Wang, Effect of the starting microstructure on the thermal properties of as-sprayed and thermally exposed plasma-sprayed YSZ coatings, J. Am. Ceram. Soc. 92 (3) (2009) 710–716.
[27] R. Vassen, N. Czech, W. Mallener, W. Stamm, D. Stover, Influence of impurity content and porosity of plasma-sprayed yttria-stabilized zirconia layers on the sintering behaviour, Surf. Coat. Technol. 141 (2-3) (2001) 135–140.
[28] G.R. Li, H. Xie, G.J. Yang, G. Liu, C.X. Li, C.J. Li, A comprehensive sintering mechanism for TBCs-Part I: an overall evolution with two-stage kinetics, J. Am. Ceram. Soc. 100 (5) (2017) 2176–2189.
[29] B. Cheng, N. Yang, Q. Zhang, M. Zhang, M. Zhang, L. Chen, G.J. Yang, C.X. Li, C.J. Li, Sintering induced the failure behavior of dense vertically crack and lamellar structured TBCs with equivalent thermal insulation performance, Ceram. Int. 43 (17) (2017) 15459–15465.
[30] P. Jiang, X.L. Fan, Y.L. Sun, D.J. Li, B. Li, T.J. Wang, Competition mechanism of interfacial cracks in thermal barrier coating system, Mater. Design 132 (2017) 559–566.
[31] L. Yang, Q.X. Liu, Y.C. Zhou, W.G. Mao, C. Lu, Finite element simulation on thermal fatigue of a turbine blade with thermal barrier coatings, J. Mater. Sci. Technol. 30 (4) (2014) 371–380.
[32] R.K. Nishihora, P.L. Rachadel, M.G.N. Quadri, D. Hotza, Manufacturing porous ceramic materials by tape casting-a review, J. Eur. Ceram. Soc. 38 (4) (2018) 988–1001.
[33] D.N. Boccaccini, H.L. Frandsen, S. Soprani, M. Cannio, T. Klemenso, V. Gil, P.V. Hendriksen, Influence of porosity on mechanical properties of tetragonal stabilized zirconia, J. Eur. Ceram. Soc. 38 (4) (2018) 1720–1735.
[34] A. Cipitria, I.O. Golosnoy, T.W. Clyne, A sintering model for plasma-sprayed zirconia TBCs. Part I: Free-standing coatings, Acta Mater. 57 (4) (2009) 980–992.
[35] G.R. Li, B.W. Lv, G.J. Yang, W.X. Zhang, C.X. Li, C.J. Li, Relationship between lamellar structure and elastic modulus of thermally sprayed thermal barrier coatings with intra-splat cracks, J. Therm. Spray Technol. 24 (8) (2015) 1355–1367.
[36] T. Liu, S.L. Zhang, X.T. Luo, G.J. Yang, C.X. Li, C.J. Li, High heat insulating thermal barrier coating designed with large two-dimensional inter-lamellar pores, J. Therm. Spray Technol. 25 (1-2) (2016) 222–230.
[37] N. Markocsan, P. Nylen, J. Wigren, X.H. Li, A. Tricoire, Effect of thermal aging on microstructure and functional properties of zirconia-base thermal barrier coatings, J. Therm. Spray Technol. 18 (2) (2009) 201–208.
[38] T. Liu, X.T. Luo, X. Chen, G.J. Yang, C.X. Li, C.J. Li, Morphology and size evolution of interlamellar two-dimensional pores in plasma-sprayed $La_2Zr_2O_7$ coatings during thermal exposure at 1300 °C, J. Therm. Spray Technol. 24 (5) (2015) 739–748.
[39] G.R. Li, H. Xie, G.J. Yang, G. Liu, C.X. Li, C.J. Li, A comprehensive sintering mechanism for TBCs-Part II: Multiscale multipoint interconnection-enhanced initial kinetics, J. Am. Ceram. Soc. 100 (9) (2017) 4240–4251.
[40] D.R. Clarke, M. Oechsner, N.P. Padture, Thermal-barrier coatings for more efficient gas-turbine engines, MRS Bull. 37 (10) (2012) 891–902.
[41] R. Vassen, Y. Kagawa, R. Subramanian, P. Zombo, D.M. Zhu, Testing and evaluation of thermal-barrier coatings, MRS Bull. 37 (10) (2012) 911–916.
[42] W.X. Zhang, T.J. Wang, L.X. Li, Numerical analysis of the transverse strengthening behavior of fiber-reinforced metal matrix composites, Comp. Mater. Sci. 39 (3) (2007) 684–696.
[43] A.J. Shaler, H. Udin, G.C. Kuczynski, M. Bever, Self-diffusion in sintering of metallic particles - discussion, T. Am. I. Min. Met. Eng. 185 (11) (1949) 896–897.
[44] G.R. Li, G.J. Yang, C.X. Li, C.J. Li, A comprehensive mechanism for the sintering of plasma-sprayed nanostructured thermal barrier coatings, Ceram. Int. 43 (13) (2017) 9600–9615.
[45] T. Liu, X. Chen, G.J. Yang, C.J. Li, Properties evolution of plasma-sprayed $La_2Zr_2O_7$ coating induced by pore structure evolution during thermal exposure, Ceram. Int. 42 (14) (2016) 15485–15492.
[46] K.A. Erk, C. Deschaseaux, R.W. Trice, Grain-boundary grooving of plasma-sprayed yttria-stabilized zirconia thermal barrier coatings, J. Am. Ceram. Soc. 89 (5) (2006) 1673–1678.
[47] C.J. Li, A. Ohmori, Relationships between the microstructure and properties of thermally sprayed deposits, J. Therm. Spray Technol. 11 (3) (2002) 365–374.